Tutorial: Least squares migration and full waveform imaging

Ian F. Jones[1]*, Carlos Calderón-Macías[2], Beng Seong Ong[2] and Ivan Berranger[2].

Abstract

A major underlying assumption of migration is that the input data are adequately sampled in terms of surface coverage. In addition, we hope that the subsurface is adequately illuminated, and that the migration algorithm itself is based on an acceptable numerical approximation of the wave equation. However, in general these assumptions and aspirations are never fully met, leading to amplitude imbalance and blurring of the output image. To some extent, this blurring and amplitude imbalance can be removed from the migrated data via application of some form of localised deconvolution, generally referred to as least-squares migration. This image modification can be performed in either the data or the image domain and can be achieved via an iterative or a single pass process, under the assumption that the velocity model is acceptable and that no coherent noise such as multiples, contaminates the input data. In this tutorial, we outline some of the various possible approaches to least-squares migration, and comment on the emerging ideas of adapting full waveform inversion to supplant some of the more expensive forms of least-squares image modification.

Introduction

Migration algorithms rely on various numerical approximations to form an image: these approximations have shortcomings which inevitably lead to noise and loss of resolution in the image. In addition, sampling irregularity can also lead to sub-optimal imaging. The idea behind least-squares (LS) migration, is to try to mitigate some of these shortcomings, so as to improve: resolution, amplitude balance, and the signal-to-noise ratio in the resulting modified image (Schuster 1997; 2017; Nemeth et al. 1999; Hu et al. 2001). A fundamental assumption of LS migration is the correctness of the model for predicting the kinematics of reflections.

The underlying idea behind all LS migration methods can be described as follows. Imagine that we have some perfect data, very densely sampled with no irregularities, no multiples, and no noise. And, if we also had a migration algorithm as a perfect inverse operator and the 'correct' velocity model, then if we migrated these data to produce an image and then de-migrated this image to create synthetic modelled pre-stack shot gathers, we would perfectly *reproduce* the original input shot gathers. Subtracting the synthetic modelled (de-migrated) data from the original data would give us a 'residual', which would be everywhere zero in this 'perfect' scenario. However, our input data are not perfectly sampled – they have gaps in the surface sampling due to acquisition limitations, variability in subsurface illumination due to refraction in the overburden, and varying amplitude due to source energy variation and receiver coupling, etc. We can now set-up an iterative inverse problem so as to minimise this residual by somehow modifying the image: in effect we are implementing a form of data regularisation and spectral shaping via inversion, so as to obtain an enhanced image in better agreement with the Earth's reflectivity. Figure 1 shows flowcharts comparing a conventional migration workflow with a LS migration workflow (Verschuur and Berkhout 2015).

It should be noted that this procedure assumes that:

1. we have an accurate velocity model in a kinematics sense, and
2. that the data are not corrupted in any way by organised coherent noise such as multiples or converted modes.

If we were to modify both the image *and* the velocity model to fit the data, this would become a form of waveform inversion, and with this in-mind, a number of techniques have been developed to separate the long wavelength (velocity-related) and shorter wavelength (reflectivity-related) updates. Examples of these are Joint Migration Inversion (JMI: e.g. Verschuur and Berkhout, 2015), the simultaneous inversion of velocity and reflectivity method of Yang et al (2021), and the scale separation waveform inversion method of Zhou et al. (2015), among others. An extension to these methods would be to work with field data including all families of multiples, and then to perform the forward modelling (demigration) with a two-way propagator so as to include multiples, and then the iterative image update would constitute a method of 'imaging with multiples', referred to as Full Wavefield Migration (FWM) in the work of Berkhout and Verschuur (1997) and Berkhout (1999; 2014).

[1] BrightSkies GeoScience | [2]formerly ION, now TGS
* Corresponding author, E-mail: ianfjones01@outlook.com
DOI: xxx

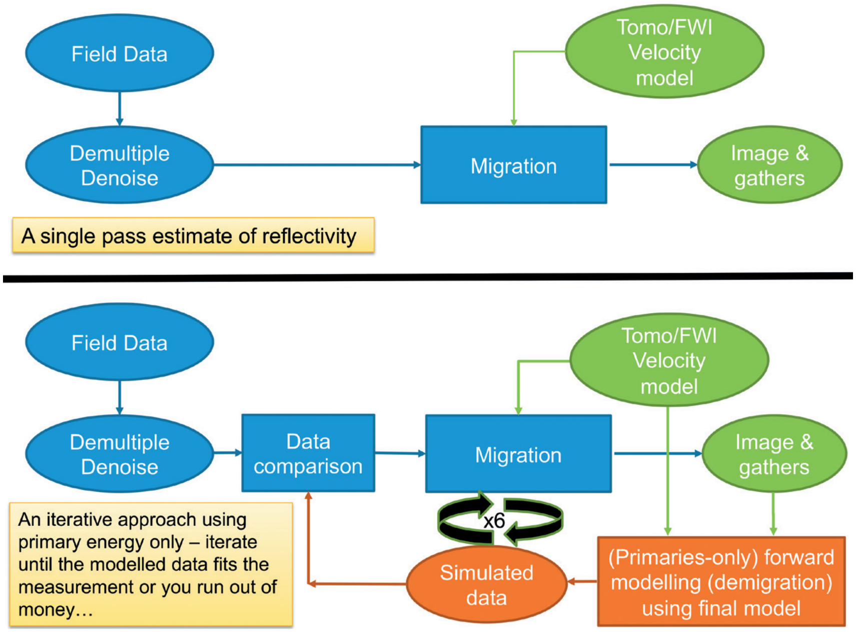

Figure 1 Top: Conventional migration. Bottom: Least Squares (primaries-only) migration

In addition to the simplified description above, we need to consider whether the residual is formed on data following migration either using, say, the standard migration image or perhaps using Common Reflection Point (CRP) gathers (image domain LS migration: e.g. Khalil et al. 2016; Fletcher et al. 2016; Lu et al., 2017) or alternatively via matching modelled data against the pre-processed shot gathers (data domain LS migration, see Appendix for more detail). The matching itself could be via an iterative procedure or a simpler and much less costly one-pass approach (Nemeth, et al. 1999; Hu et al. 2001; Guitton, 2004).

The procedure of LS migration is performed only on a final production image after completion of all velocity model updates (as we assume that the model is 'perfect'), and the procedure of LS modification of this final image can be applied to any form of migrated image, e.g. time migration, Q-migration, Kirchhoff depth migration (Casasanta et al., 2017), RTM (Wong, 2013; Zhang et al., 2015; Wang et al., 2016; Fletcher and Cavalca, 2018), etc. Perhaps it is better thought of as an LS *modification* of an *existing* image, rather than as a form of migration in itself. Importantly, note that LS migration *cannot* improve the structure of the image itself, as there is no change in the position of events: it is only the amplitude balance (and corresponding illumination), resolution, and SNR that the LS modification can hope to improve.

Table 1 summarises the various options available for performing the LS modification of an existing image. The first step for all methods is to take the final production migration stacked image, and to demigrate it with the velocity model used to form this production migration as input. This creates a set of synthetic shot gathers. The synthetic computation uses the shot and receiver locations used in the migration of the field data, with or without source and receiver regularisation. A formal mathematical representation of these procedures is outlined in Appendix 1. In the following sections, we will expand on the image and data domain LS migration options and some of its main practical aspects.

Image domain LS migration

Migrate the synthetic shot gathers to form synthetic CRP gathers. It is important to note that these CRP gathers will be perfectly flat as they were migrated with the velocities used to create them. However, any residual velocity error in the final velocity model being used in the procedure will have given rise to real CRP gathers that were not perfectly flat. This mis-match between the field data CRPs and the synthetic CRPs will be discussed later. If using a stacked image from field data to act as reflectivity model for the forward modelling (to create the synthetic shot gathers), we need to ensure that the image being used is 'clean' and well sampled. This might thus require some image post-processing to remove noise. To prevent spatial aliasing for the dips and bandwidth

Image domain Post-stack	Image domain Pre-stack	Data domain Pre-stack
Migrate the synthetic shot data to form synthetic CRP gathers and stack them. In small overlapping windows, create shaping filter operators to make the synthetic image resemble the target image. Apply these shaping operators to the real image, so as to 'de-blur' the field image. Single iteration approach.	In small overlapping windows, create shaping operators to make each individual offset image resemble the target image. Apply the operators to each offset class independently. By using the same target image for all offsets, we avoid introducing spurious AVO effects. Single iteration approach.	Subtract the field data shot gathers from the synthetic (modelled) shot gathers to form a residual. Migrate this residual and subtract a scaled version of this 'residual image' from the original field data migrated image. This procedure closely resembles FWI, but here we are updating the image rather than the associated velocity. Performed with one or more iterations.

Table 1 Additional steps involved in an LS procedure, after demigration (forward modelling) using the production migration image as the reflectivity model.

being modelled, some interpolation of the traces in the image might be required. These procedures will be designed to ensure that the modelled (synthetic) shots are free of numerical artefacts.

The synthetic CRP gathers are now stacked to form a synthetic image, and shaping operators designed in small overlapping windows are applied to make the synthetic image look like the target image: these operators can be thought of as deblurring filters. These operators are now applied to the original field data image, and if all is working well the effect will be to enhance resolution and suppress noise in the field data image. There are different choices for the target image, such as the field migrated stack as previously described. Another choice corresponds to the use of a volume with regularly sampled point spread functions (PSF's: e.g. Fletcher et a., 2016). The LS workflow is independent of the choice of target image, which is also independent of the background velocity which is assumed to be a smooth model. The selection of target reflectivity with PSFs or a migrated field image might produce slight differences depending of the geology being treated as well as specific characteristics of the filters being used (e.g., Aoki and Schuster, 2009; Wang et al. 2017). Guitton (2004) proposed the use of nonstationary matching filters (to approximate the inverse Hessian in a single iteration: see equation A4 in the Appendix), which are derived and applied spatially in overlapping windows, whereas Wang et al. (2017) proposed the derivation of the filters in the curvelet domain as a way to better separate illumination direction and frequency scale in the image when matching the field and the synthetic image.

If working directly on the CRP gathers (pre-stack image domain LS modification) then the adaptation filters can be computed for each offset volume independently. For a stack or for each offset volume, the compute cost of LS migration in the image domain is about two to three times that of a standard migration, with the modelling step accounting for most of the cost (computation of filters is a small percentage of the total cost). The Appendix describes equations for filter derivation.

Data domain LS migration

This is a more contentious procedure, because if we want to compare pre-stack field data with modelled data, we need to consider any true AVO effects in the field data (so as to preserve such behaviour, e.g. Kuhl and Sacchi 2003), and this would require an elastic migration and demigration procedure, plus a description of the elastic properties. For image domain LS methods, this aspect is not an issue, as we are simply comparing acoustic migrated field data with synthetic acoustically modelled and migrated data.

As outlined in Table 1, one method would be to subtract the field data shot gathers from the synthetic (modelled) shot gathers to form a residual. Then we migrate this residual, and subtract a scaled version of this 'residual image' from the original field data migrated image (and iterate if desired). Alternatively, we could create shaping operators to make the synthetic traces resemble the real traces, then apply these operators to the synthetic traces and migrate them. Equation A1 in the Appendix describes the LS migration in the data domain.

Compared to the cost of LS migration in the image domain, the data domain approach is much more costly due to its iterative nature, and comparison of the two approaches (Fletcher et al., 2016) suggests that the image domain method could achieve comparable or better results in a subsalt scenario. This can be related to the locality of the filters in the image domain approach and the simplicity and high efficiency for readjusting filter characteristics (Fletcher et al., 2016) without the need to remodel and remigrate the data. Nevertheless, there are some cases that cannot be treated in the image domain such as reducing artifacts when migrating multiples (e.g., Wong et al., 2014) as well as reducing sampling artifacts with LS migration. For these cases, the data domain approach is a better solution although its use has not been widespread due to its cost and other limiting factors such as the use of inaccurate physics.

Iterative versus non-Iterative methods

This comes down to cost: each iteration of the LS modification costs the same (about twice the cost of a basic migration, as each iteration requires a demigration of the input plus a remigration of the created synthetic data). It can be observed that most of the desired image improvement comes from the first few iterations of an iterative LS migration, but most of the uplift is obtained in just the first iteration: hence the interest in a cheaper single-pass approach. The design of the iterative strategy could simply be to repeat the method used in the original single pass, or employ a more elegant LS minimisation of the residual (e.g. Duan et al., 2020). Here the residual would be formed from the difference between the previous de-blurred real data and the current synthetic data. A hybrid scheme could use a first pass of deblurring operators obtained in the image domain and a single pass of a data domain step (e.g., Aoki and Schuster, 2009).

Presence of velocity error

Given that the LS techniques assume that the migration velocity model is perfect, then in an image domain LS scheme the synthetic CRP gathers produced in the demigration and subsequent remigration will be perfectly flat. If we compared these gathers to the real (and not perfectly flat) CRP gathers and derived the LS shaping operators, we would introduce a peculiar error which would vary throughout the data depending on how non-flat the real CRP gathers were. Hence, in the presence of velocity error, the LS modification can actually degrade the result. One approach towards circumventing this problem would be to apply the shaping operators to individually processed offset volumes, thus preserving the (non flat) RMO behaviour in the gathers (e.g. Wang et al., 2020; Shadrina et al., 2020), and/or use large probe windows in the computation of the filters so as to avoid localised velocity uncertainties. A bigger problem appears when the velocity model contains high contrast layers, such as the presence of a salt body, which might have been erroneously located in the model from interpretation due to lack of signal. In this particular case, unwanted 'signal' might be introduced in the LS migrated result. A solution to this problem is to avoid computation of filters in these regions (e.g., Fletcher and Cavalca, 2018).

Attenuation considerations

For dealing with attenuation (Q), there are differing ways to approach the problem. If we had used a conventional (non-Q-compensating) migration algorithm to create the initial image, then we could perform regular LS modification with a corresponding non-Q demigration/remigration scheme. This would be self-consistent, and leave us no worse off than before, but if there were significant attenuation issues in the data, these would still need to be dealt with using some form of Q compensation before or after migration. By performing the LS migration having ignored Q effects, we would at least have dealt with all the other aforementioned problems that LS migration tries to address. Alternatively, we could employ a true Q-migration scheme (e.g. da Silva et al., 2020) and a corresponding Q-demigration to go with it (e.g. Dutta and Schuster 2014; Cavalca et al., 2015; 2016). In addition, intermediate routes could also be followed, wherein we used a Q-migration, but then employed a (non-Q) demigration for the modelling phase of the LS procedure. The rationale for this latter (apparently contradictory) route is that the initial Q-migration will have removed the earth attenuation effects from the initial image, and thereafter we can justify using a non-Q demigration, thereby relying on the LS procedure to compensate for the more usual migration shortcomings (e.g. Chen et al., 2019).

Full waveform inversion imaging

Currently, LS migration is used on many, but not all, imaging projects, and could thus be viewed as being almost at the point of being mainstream, established, routine technology. However, given some recent developments in FWI imaging (Appendix 1) it could be suggested that LS migration methods will become obsolete before they get to become routine. Given that the Earth's reflectivity structure is related to impedance contrasts across reflecting layer boundaries, then assessing the changes in velocity across these boundaries can be used as a proxy for reflectivity if combined with some estimate of the associated density changes. Thus, taking the derivative (normal to the layer boundaries) of a high frequency FWI velocity model and scaling with a density proxy can produce an emulation of the Earth's reflectivity structure (Zhang et al., 2020): see equations A6-A11 in the Appendix for the derivation of the FWI image from the estimated velocity. Nevertheless, more accurate physics for the propagators as well as better constraints for properties such as density and shear wave velocity are still required for separating acoustic and elastic effects and producing a more geologically accurate image. We note that the synthetics used for LS migration are computed with Born modelling or de-migration, while most FWI work uses full wave modelled synthetics in which interfaces are embedded in the velocity model.

Given that FWI using a two-way propagator (such as used in RTM) can in principle model all classes of multiples, the

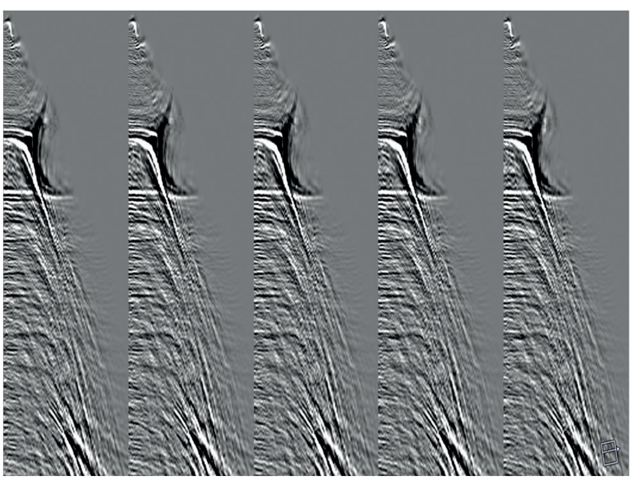

Figure 2 Field data Kirchhoff CRP gathers.

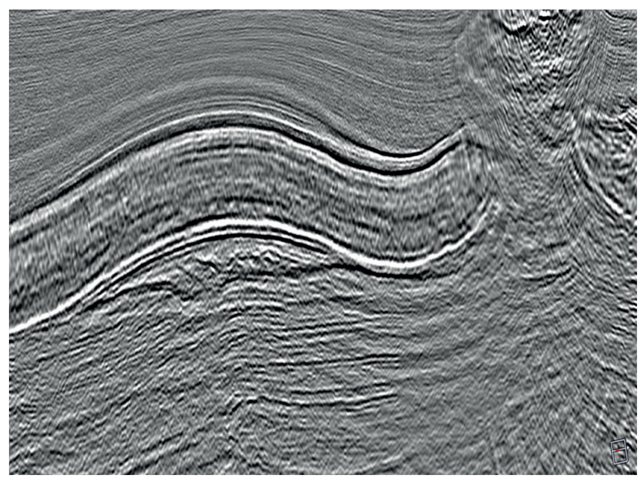

Figure 4 Field data Kirchhoff preSDM stack.

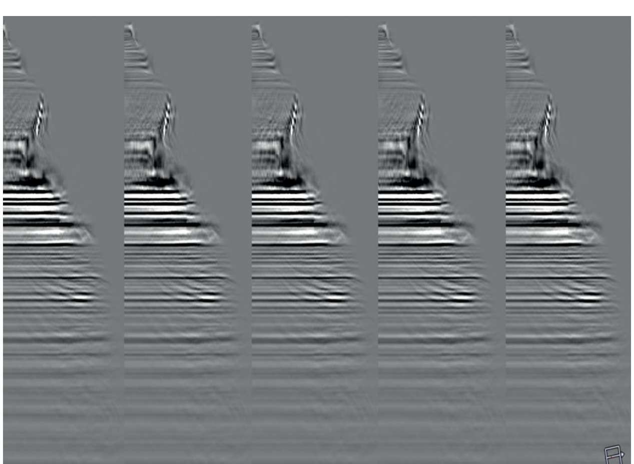

Figure 3 Synthetic modelled CRP gathers: note the absence of noise and perfect gather flatness.

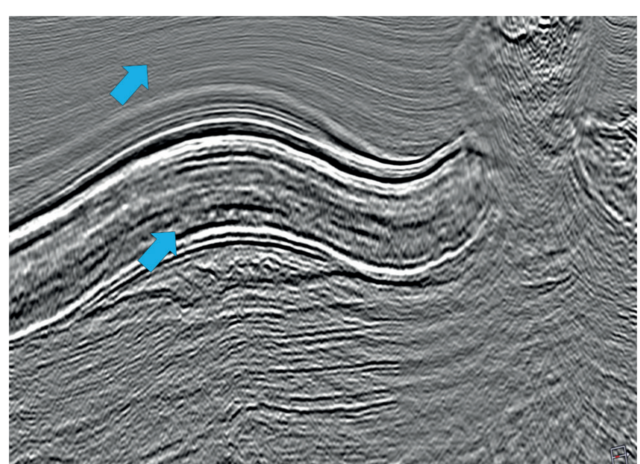

Figure 5 LS Kirchhoff preSDM. Arrows point at evident improvement areas in the image.

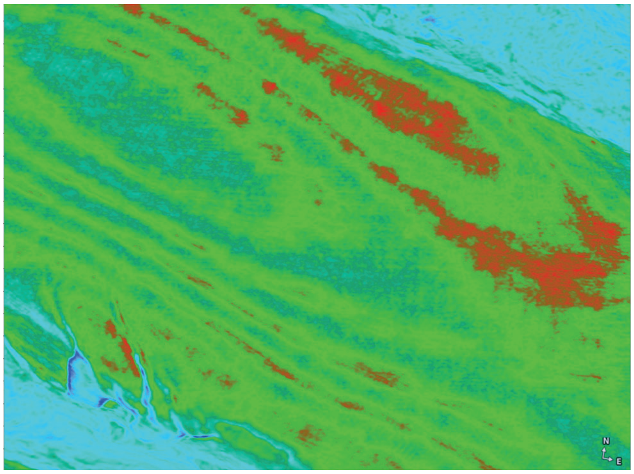

Figure 6 Amplitudes on a target horizon from field data Kirchhoff preSDM stack.

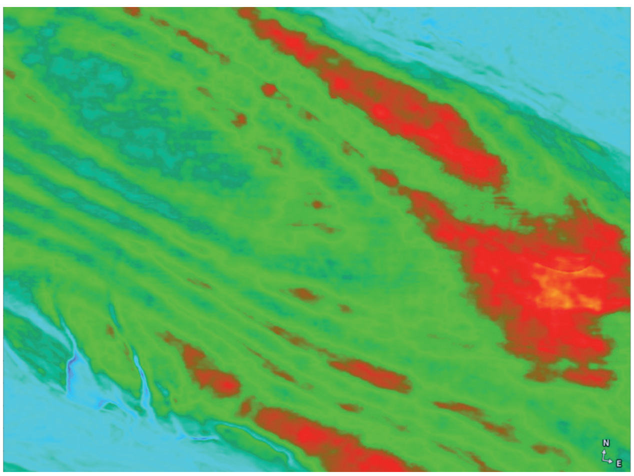

Figure 7 Amplitudes on the target horizon from LS preSDM stack.

velocity model estimated using FWI can make use of the modelled multiples in estimating this model. In addition, noting that multiples tend to have more vertical angles of incidence tham the associated primary reflections, an image obtained using multiples and primaries should have higher vertical resolution than a 'primaries-only' image. Also, and perhaps more importantly, FWI uses various forms of regularisation to constrain the result of the underlying data-domain velocity inversion with assorted image domain (model) constraints. Such constraints can include perturbation smoothing using the structural tensor (Hale, 2009), or a total variation norm (Anagaw and Sacchi, 2011). These constraints tend to reduce the classical migration noise which is present in the FWI gradient and visible in conventional migration results, such that the FWI velocity field is more 'noise-free' than the associated migrated image. Hence, if we derive an image by taking the derivative of the velocities (along a direction normal to the structural interfaces) we will most likely obtain a cleaner and better resolved image than that obtained from the corresponding conventional migration. However, in order for the modelling to reproduce a given class of multiples (such as the 'interbeds'), the multiple-generating layers must have been successfully incorporated into a mostly correct velocity model during FWI. As has been demonstrated in recent FWI applications, availability of ultra-low-to-low frequencies, long to ultra-long offsets and rich azimuth coverage are all important for deriving an accurate velocity model. Hence, it is expected that the more accurate and better resolved FWI images utilise data acquired with all or some of these characteristics. The downside of high-resolution imaging with FWI is the associated cost: in order to obtain an image with a comparable bandwidth to a conventional migration, we need to run the FWI to a comparably high frequency, which is costly. However, if we did this, the image so derived could be thought of as an LS RTM with regularisation-constraint smoothing which

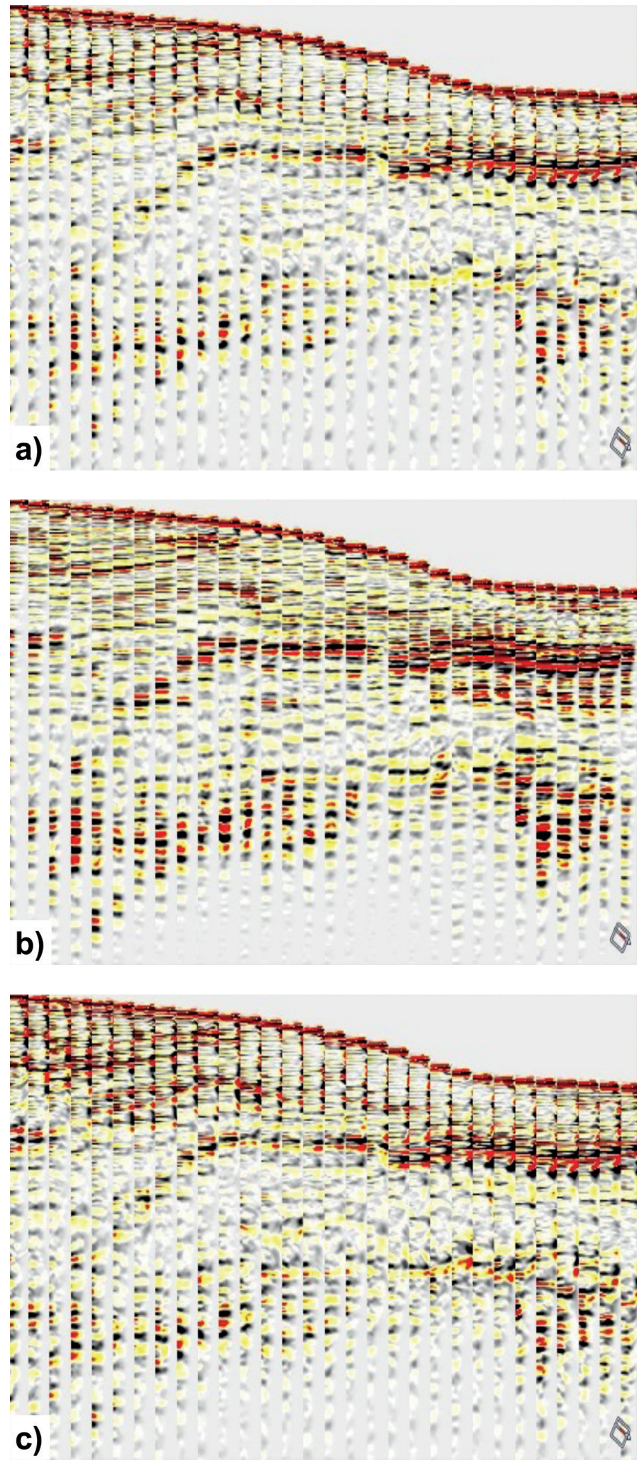

Figure 8 a) Field RTM angle gathers. b) Synthetic RTM angle gathers. c) LS RTM angle gathers.

had incorporated the contribution of (the modelled) multiples in deriving the image. LS migration specially in the image domain, will likely still be a viable solution for improving a standard image given its reduced cost compared to its data domain counterpart and to imaging with FWI.

Examples

We present two examples that display some of the benefits of applying LS migration in the image domain using local matching filters. The standard field data image with little post-processing is used as target reflectivity. In both cases, LS migration is performed with a high-quality velocity model that produces flat common image gathers and a final migrated stack with little post-processing. The choice of using image domain versus data domain is driven by efficiency given project size and the relatively high frequency being targeted. We have found that using the migrated field stack as target reflectivity, as opposed to PSFs, has advantages for QCing the results, since the synthetic and field images can be compared against each other to determine areas of improvement as well as potential problems such as numerical artifacts introduced by the modelling.

It should also be noted, that any non-primary energy in the field data (such as multiples, converted modes, and other coherent noise) will tend to degrade the synthetic modelled data: consequently, some judicious additional filtering of the input field data can sometimes be advisable.

In the first example, a streamer narrow-azimuth (NAZ) dataset is imaged with a TTI Kirchhoff migration. Figure 2 shows the real migrated CRP gathers and Figure 3 a re-migration of synthetic gathers modelled with a Kirchhoff scheme. Key factors of the modelling are the handling of antialiasing and the control of amplitudes from the ray tracing. Notice that the remigrated gathers show signal all the way out to the maximum offset and perfectly aligned events since modelling and migration operations rely on the same velocity model. Furthermore, noise observed in the field data such as residual surface related multiples, internal multiples and mode conversions are not present in the synthetic migrated gathers which are much cleaner. The main purpose of applying the LS migration in this project is to extend continuity of reflectors and reduce the potential of amplifying high frequency noise from the raw image, achieved by using relatively large image sub-volumes and optimising the filter length.

Least-squares filters are obtained as an illumination compensation correction associated with blurring resulting from the migration operation. The filters can be designed to target the higher SNR and event continuity in the section, and target some of the noise in their application. It is easier to see the advantages of LS migration in this example by comparing the field migrated stack before and after application of the filters in the individual offsets (Figures 4 and 5 respectively). The arrows in Figure 5 point to areas in the stack where improvements in SNR are observed, mostly in reducing high-frequency noise and improving event continuity. We want to apply LS migration filters to relatively raw gathers without a denoise process that potentially eliminates high frequencies, so any additional processing, such as remnant multiple suppression, can be applied following the LS modification. The reduction of noise and improved illumination of the LS migration can be better observed in an amplitude slice extracted from an interpreted horizon, as shown in Figures 6 and 7. Additional denoise and multiple suppression were also performed on both the original and the LS migrations.

In the second example, a 45 Hz RTM stack of a NAZ dataset after processing is used as the pilot reflectivity to generate synthetic seismograms that are then migrated for computing 3D filters as in the previous example. The main expectation of using LS migration in this project is to improve the amplitudes of both the gathers and image due to variations in illumination, and a secondary objective is to extend the bandwidth of the signal for both sediments and pre-salt sections. The CRP gathers of the field data are shown in Figure 8a and the synthetic gathers are shown in Figure 8b. For this example, LS filters were estimated per angle-class with the field RTM stack used as the target image. To preserve signal and amplitude variations with angle, the filters are designed and applied for each angle-class independently (Figure 8c). It is also possible to design the filters using partial angle stacks and then apply the filters on individual angles. In our testing, we have not seen an advantage in doing so (not shown here for brevity), but it is expected that this is signal dependent and there might be individual angle sections with poor SNR due

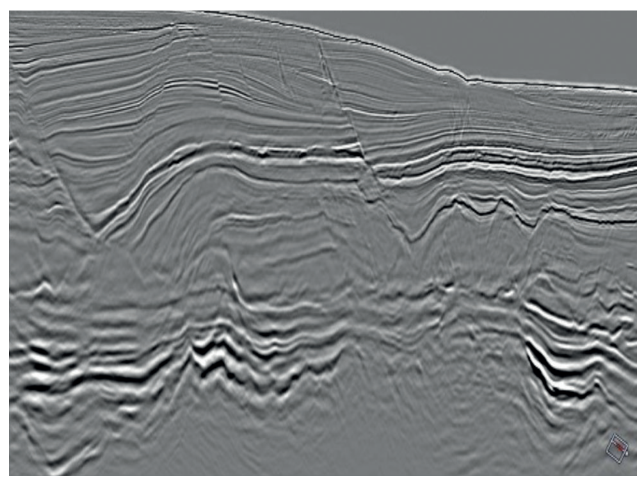

Figure 9 Field RTM stack. The stack is used as reflectivity image for generating synthetic seismograms.

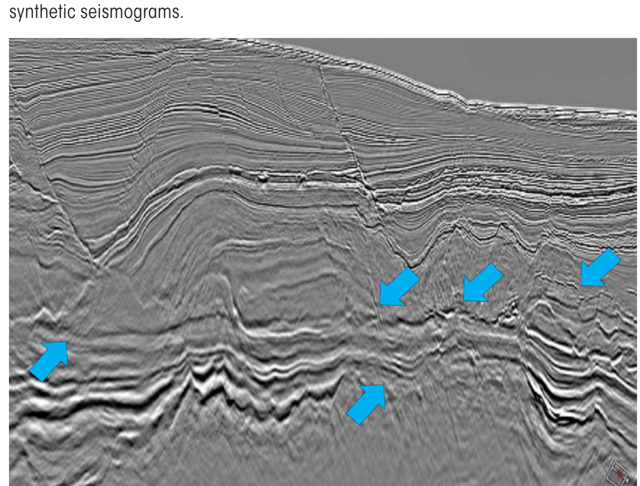

Figure 10 Stack of LS RTM angle gathers. Arrows mark areas of improved illumination.

to poor illumination and poor data sampling. Another characteristic of our implementation is in adjusting filter parameters such as probe size and filter length spatially. This is needed because of expected variations of SNR mostly with depth and frequency. Figure 9 shows the field data RTM stack and Figure 10 the image resulting from stacking the LS RTM angle gathers from Figure 8c. Comparing these stacks, the most noticeable effect corresponds to an extended bandwidth of the LS RTM image, also seen in the spectra plots of Figure 11. Notice the higher bandwidth enhancement in the horizontal direction (Figure 11c).

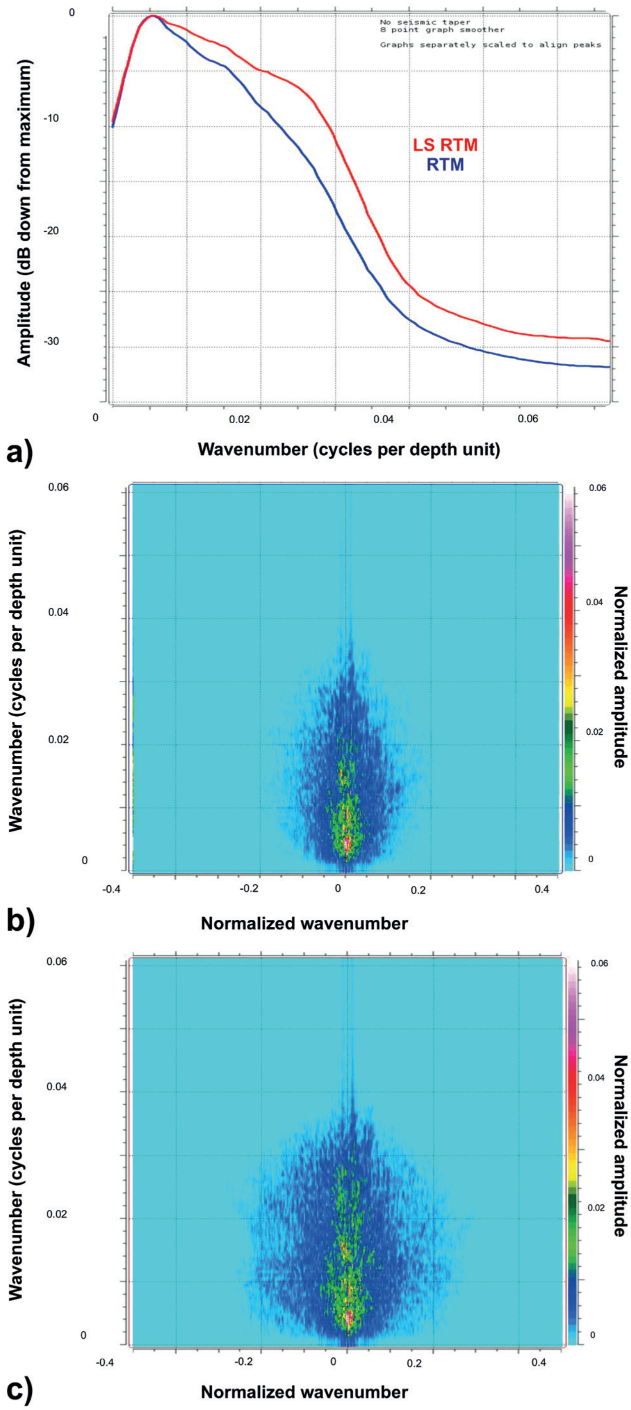

Figure 11 a) Amplitude spectra of input RTM stack (red) and LS RTM stack (blue). b) Wavenumber plot for RTM stack. c) Wavenumber plot for LS RTM stack.

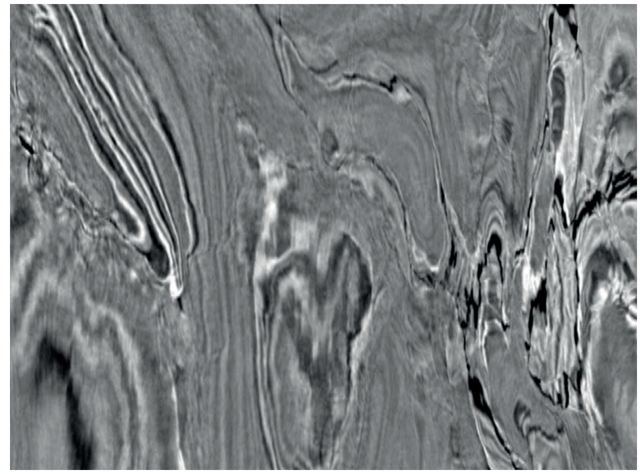

Figure 12 Horizontal slice at intermediate depth from field RTM stack.

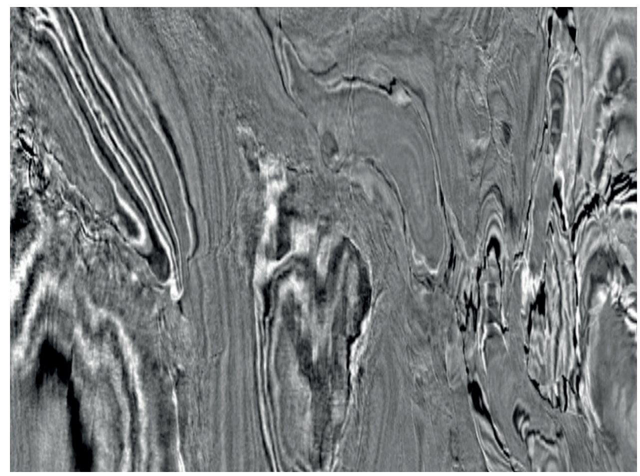

Figure 13 Corresponding slice from LS RTM stack.

The blue arrows in Figure 10 point to areas of better illumination after LS migration. Figures 12 and 13 show horizontal slices in the sedimentary section at an intermediate depth in the image, for the field RTM stack and LS RTM result. The most noticeable effects are the enhanced resolution and a slight improvement in amplitudes depicting an improved amplitude balance laterally. Although differences are relatively small, the LS migrated image helps interpretability of events and makes it an overall better product for amplitude analysis.

Conclusions

Least-squares modification of a migrated image can provide better resolution and a cleaner image than that obtained in a conventional migration. A single-pass approach can prove to be a very cost effective way to enhance a migration. LS migration in the image domain is preferred over the data domain approach in the industry due to its higher benefit over cost ratio. LS imaging can be employed for any migration algorithm in time or depth domain, post- or pre-stack migration, ray or wave equation-based migration. However, given the emergence of FWI-imaging, data-domain LS migration as a thing in itself might become obsolete before it becomes fully established. But, it should be remembered that the LS minimisation methodology is in fact being used within full waveform inversion, hence the principles of LS inversion are still being employed, albeit in a slightly different guise. Through this optic, LS migration can be viewed as being extended rather than becoming obsolete.

Acknowledgements
We would like to thank Valter Marquez, Bianca Bianchi and Juergen Fruehn for their work on the examples shown, Clement Kostov, John Brittan, and other reviewers for helpful suggestions with the manuscript, and Vaalco and Petrobras for permission to show the field data examples.

References

Anagaw, A.Y. and Sacchi, M.D. [2011]. Full Waveform Inversion with Total Variation Regularization. *CSPG CSEG CWLS Convention.*

Aoki, N. and Schuster, G.T. [2009]. Fast least-squares migration with a deblurring filter: *Geophysics*, **74**(6), WCA83-WCA92.

Berkhout, A.J. [1999]. Multiple removal based on the feedback model: *The Leading Edge*, **18**, 127-131.

Berkhout, A.J. and Verschuur, D.J. [1997]. Estimation of multiple scattering by iterative inversion — Part I: Theoretical considerations: *Geophysics*, **62**, 1586-1595.

Berkhout, A.J. [2014]. Review Paper: An outlook on the future of seismic imaging, Part III: Joint Migration Inversion: *Geophisical Prospecting*, **62**, 950-971.

Casasanta, L., Roberts, G., Perrone, F., Ratcliffe, A., Poole, G., Wang, Y. and Xie, Y. [2017]. Practical benefits of Kirchhoff Least-squares Migration Deconvolution. *79th EAGE Conference and Exhibition, Extended Abstracts.*

Cavalca, M., Fletcher, R.P. and Du, X. [2015]. Q compensation through depth domain inversion. *77th EAGE Conference & Exhibition, Extended Abstracts.*

Cavalca, M, Fletcher, R.P. and Caprioli, P. [2016]. Least Squares Kirchhoff Depth Migration in the image domain. *78th EAGE Conference & Exhibition, Extended Abstracts.*

Chen, Y., Guo, B. and Schuster, G.T. [2019]. Migration of visco-acoustic data using acoustic reverse time migration with hybrid deblurring filters: *Geophysics*, **84**(3), S127-S136.

Da Silva, N. Casasanta, L. and Grion, S. [2020]. QRTM – Stable and effective anelastic loss compensation, *82nd EAGE Conference and Exhibition, Extended Abstracts.*

Duan, L., Valenciano, A. and Chemingui, N. [2020]. Iterative least-squares migration for high-resolution angle gathers, *90th SEG Annual International Meeting, Expanded Abstracts.*

Dutta, G. and Schuster, G.T. [2014]. Attenuation compensation for least-squares reverse time migration using the viscoacoustic-wave equation, *Geophysics*, **79**, S251-S262.

Fletcher, R.P., Nichols, D., Bloor, R. and Coates, R.T. [2016]. Least-squares migration – Data domain versus image domain using point-spread functions. *The Leading Edge,* **35**, 157-162.

Fletcher, R. and Calvalca, M. [2018]. Improving imaging-domain least-squares reverse time migration close to high velocity contrasts, *80th EAGE Conference and Exhibition, Extended Abstracts.*

Gardner, G.H.F., Gardner, L.W. and Gregory, A.R. [1974]. Formation velocity and density - the diagnostic basics for stratigraphic traps. *Geophysics*. **39**, 770-780.

Guitton, A. [2004]. Amplitude and kinematic corrections of migrated images for nonunitary imaging operators. *Geophysics*, **69**, 1017-1024.

Hale, D. [2009]. Structure-oriented smoothing and semblance. *CWP Report 634. https://inside.mines.edu/~dhale/papers/Hale09StructureOrientedSmoothingAndSemblance.pdf.* Accessed January 2023.

Hu, J., Schuster, G.T. and Valasek, P. [2001]. Poststack migration deconvolution. *Geophysics*, **66**, 939-952.

Huang, S., Wang, M., Bai, B. and Wang, P. [2017]. Improving subsalt imaging with least-squares RTM – A case study at Kaskida Field, Gulf of Mexico. *79th EAGE Conference and Exhibition, Extended Abstracts.*

Khalil, A., Hoeber, H., Roberts, G. and Perrone, F. [2016]. An alternative to least-squares imaging using data-domain matching filters. *86th SEG Annual International Meeting, Expanded Abstracts.*

Kuhl, H. and Sacchi, M.D. [2003]. Least-squares wave-equation migration for AVP/AVA inversion, *Geophysics*, **68**, 262-273.

Liu, J, Yang, M., Deeds, J., Luckow, J., Cheriyan, T., Ariston, P-O., Yang, Z., Mei, M. and Zhang, Z. [2021]. Solving subsalt imaging challenges in Green Canyon using OBN and FWI Imaging. *91st SEG Annual International Meeting, Expanded Abstracts.*

Lu, S., Li, X., Valenciano, A., Chemingui, N. and Cheng, C. [2017]. Least-squares wave-equation migration for broadband imaging. *79th EAGE Conference and Exhibition, Extended Abstracts.*

Nemeth, T., Wu, C., and Schuster, G. T. [1999]. Least-squares migration of incomplete reflection data: *Geophysics*, **64**, 208-22.

Salaun, N., Reinier, M., Espin, I., and Gigou, G. [2021]. FWI velocity and imaging: a case study in the Johan Castberg area. *First Break,* **39**(12), 45-54.

Schuster, G. [1997]. Acquisition footprint removal by least square migration: *1997 Annual UTAM Report,* 73-99.

Schuster, G.T. [2017]. Seismic Inversion. *Investigations in Geophysics,* **20**, SEG, Tulsa.

Shadrina, M., Cavalca, M., Ortin, M., Pantoja, M., Medina, E., Leone, C. and Fletcher, R. [2020]. Prestack least-squares RTM on surface offset gathers for more reliable interpretation – Santos Basin case study. *90th SEG Annual International Meeting, Expanded Abstracts.*

Verschuur, D.J. and Berkhout, A.J. [2015]. From removing to using multiples in closed-loop imaging. *The Leading Edge,* **34** (7), 744–759.

Wang, P., Gomes, A., Zhang, Z. and Wang, M. [2016]. Least-squares RTM: Reality and possibilities for subsalt imaging. *86th SEG Annual International Meeting, Expanded Abstracts.*

Wang, M., Xu, S., Zhou, H., Tang, B., DeNosaquo, A., and Ionescu, G. [2020]. Efficient Gather Domain Least-Squares Reverse Time Migration for Inaccurate Velocity Models. *82nd EAGE Conference and Exhibition, Extended Abstracts.*

Wang, B., He, Y., Mao, J., Liu, F., Hao, F., Huang, Y., Perz, M. and Michell, S. [2021]. Inversion-based imaging: from LSRTM to FWI imaging. *First Break,* **39**(12), 85-94.

Wong, M. [2013]. Handling salt reflection in least-squares RTM. *83rd SEG Annual International Meeting, Expanded Abstracts.*

Wong, M., Biondo, B.K. and Ronen, S. [2014]. Imaging multiples using least-squares reverse time migration, *The Leading Edge*, **33**, 970-976.

Yang, Y., Ramos-Martinez, J., Whitmore, D., Huang, G., and Chemingui, N. [2021]. Simultaneous inversion of velocity and reflectivity, *First Break*, **39**, 55-59.

Zhang, Y., Duan, L., and Xie, Y. [2015]. A stable and practical implementation of least-squares reverse time migration. *Geophysics*, **80**, 23-v31.

Zhang, Z., Wu, Z., Wei, Z., Mei, J., Huang, R. and Wang, P. [2020]. FWI Imaging: Full-wavefield imaging through full-waveform inversion. *90th SEG Annual International Meeting, Expanded Abstracts.*

Zhou, W., Brossier, R., Operto, S., Virieux, J. [2015]. Full waveform inversion of diving and reflected waves for velocity model building with impedance inversion based on scale separation, *Geophysical Journal International,* **202**, 1535-1554.

Appendix 1

Formal description of least squares image modification and FWI imaging (assuming linear operators)

Given the following definitions:
Migration operator: L^t ,
Modelling operator: L (which is the adjoint of L^t) ,
Hessian operator: $L^t L$,
Recorded field data shot records: d_{field} ,
Initial image from the field data: $m_0 = L^t d_{field}$,
Synthetic shot gathers created from the initial image: Lm_0 ,
Residual shot gathers: $\Delta d_n = (d_{field} - Lm_0)$.

Data domain LS migration:

The data domain LS migration m_n, for the $(n+1)^{th}$ iteration ($n = 0, 1, 2 \ldots$), can be written as:

$$m_n+1 = m_n + \alpha L^t \Delta d_n \quad \text{A1}$$

Where α is a perturbation steepest descent constant.

For an RTM algorithm, this LS modification can be formulated as a variation on FWI wherein the residual is backpropagated to form a gradient, which is then used to drive an image update rather than a velocity update.

Image domain LS migration:

If we are working with data after multiple suppression, then we only want to model primaries in the synthetic data, hence we can use, for example, single-scattering Born modelling to work with the migration velocity field and the raw migration image, m_0, to obtain synthetic data d_1:

$$d_1 = Lm_0 \quad \text{A2}$$

We can then re-migrate these data to obtain a new image m_1

$$m_1 = L^t d_1 ,$$
$$m_1 = L^t L\, m_0 \quad \text{A3}$$

Where $L^t L$ is the Hessian operator, which we can approximate by designing matching filters, f, that turn the raw migration image (m_0) into a least-squares image (m_{LS}). For this, we minimize the cost-function:

$$\min_f \| f * m_0 - m_1 \|^2 + \varepsilon \| \nabla f \|^2 \quad \text{A4}$$

Where ε is a regularization coefficient and f the matching filter which is solved through an iterative method, and then apply the derived operators, f, to the field raw migration, m_0, to obtain the image domain LS migration:

$$m_{LS} = f^* m_0 \quad \text{A5}$$

Full waveform inversion imaging.

Recall that the observed reflectivity is a manifestation of impedance contrasts at subsurface lithological interfaces (where impedance, I, is the product of density and interval velocity):

$$R = (\rho_2 v_2 - \rho_1 v_1)/(\rho_2 v_2 + \rho_1 v_1) \quad \text{A6}$$

Hence a subsurface image can be represented by the change in impedance for zero angle of incidence at a dipping layer, and can be written as:

$$Image \sim \partial I/\partial n . \quad \text{A7}$$

Where n represents the normal direction. This can be rewritten in terms of local dips as:

$$\partial I/\partial n = \rho \{ \partial v/\partial x \, Sin(\theta) \, Cos(\varphi) + \partial v/\partial y \, Sin(\theta) \, Sin(\varphi) + \partial v/\partial z \, Cos(\varphi)\} . \quad \text{A8}$$

Where ρ is the average density across the layer, θ is the dip, and φ is the azimuth of the normal vector (e.g. Zhang, et al. 2020).

Alternatively, for clastic sediments, we could use the Gardner relationship (Gardner et al., 1974) to approximate density:

$$\rho = 0.31\, v^{0.25} \quad \text{A9}$$

Where v is the P-wave interval velocity measured in m/s, and substituting into A6 obtain:

$$R = (v_2^{1.25} - v_1^{1.25})/(v_2^{1.25} + v_1^{1.25}) \quad \text{A10}$$

Setting $w=v^{1.25}$ and using the chain rule, then gives:

$$\partial I/\partial n = \rho \{ \partial v/\partial x \, Sin(\theta) \, Cos(\varphi) + \partial v/\partial y \, Sin(\theta) \, Sin(\varphi) + \partial v/\partial z \, Cos(\varphi)\} / \{1.25\, v^{0.25}\} . \quad \text{A11}$$

Again, where $w=v^{1.25}$.

However, in order to obtain a useful image, the velocities being used must be estimated with a frequency staging strategy that avoids cycle skipping, before introducing high wavenumbers into the inversion. An example of this can be found in: Zhang et al., 2020; Liu et al., 2021; Salaun et al., 2021; and Wang et al., 2021.